



HAL
open science

Passive vibration control of a beam modeled through Generalized Beam Theory using a Nonlinear Energy Sink under different loading scenarios

Andrea de Flaviis, Alireza Ture Savadkoohi, Daniele Zulli

► To cite this version:

Andrea de Flaviis, Alireza Ture Savadkoohi, Daniele Zulli. Passive vibration control of a beam modeled through Generalized Beam Theory using a Nonlinear Energy Sink under different loading scenarios. *European Journal of Mechanics - A/Solids*, 2025, 111, pp.105552. 10.1016/j.euromechsol.2024.105552 . hal-04862371

HAL Id: hal-04862371

<https://hal.science/hal-04862371v1>

Submitted on 6 Jan 2025

HAL is a multi-disciplinary open access archive for the deposit and dissemination of scientific research documents, whether they are published or not. The documents may come from teaching and research institutions in France or abroad, or from public or private research centers.

L'archive ouverte pluridisciplinaire **HAL**, est destinée au dépôt et à la diffusion de documents scientifiques de niveau recherche, publiés ou non, émanant des établissements d'enseignement et de recherche français ou étrangers, des laboratoires publics ou privés.

Passive vibration control of a beam modeled through Generalized Beam Theory using a Nonlinear Energy Sink under different loading scenarios

Andrea De Flaviis^{a,b,*}, Alireza Ture Savadkoohi^b, Daniele Zulli^a,

^a*Department of Civil, Construction-Architectural and Environmental Engineering, University of L'Aquila, Piazzale Pontieri, Loc. Monteluco, L'Aquila, 67100, Italy*

^b*ENTPE, École Centrale de Lyon, CNRS, LTDS, UMR5513, Vaulx-en-Velin Cedex, 69518, France*

Abstract

In the present paper a beam, part of a box girder bridge, modeled through Generalized Beam Theory is studied. In particular, vibrations are controlled by using a Nonlinear Energy Sink for different types of external loads. The objective is to combine this refined theory, which enables to consider interesting aspects of Thin-Walled Beams, with the concept of vibrations control through nonlinear devices, to take into account real scenarios where the use of classical beam theories and linear dampers could not be sufficient. The fundamental aspects of Generalized Beam Theory are first introduced, identifying its two main phases, cross-section analysis and member analysis, then Complexification Averaging and Multiple Scales Method are used to study the nonlinear problem, where the nonlinearity is represented by the cubic stiffness of the Nonlinear Energy Sink. Different load conditions are investigated, including earthquake and moving loads, and it is found that energy is correctly transferred from the beam to the device and, thanks to Generalized Beam Theory, vibrations due to resonant loads, with frequencies which cannot be found with classical beam theories, can be reduced. It is found that the use of a Nonlinear Energy Sink on a Thin-Walled Beam allows to reduce the vibrations even for complex loading cases, and GBT appears to be a very valuable tool in assessing this aspect. Results obtained in this

*Corresponding author

Email address: andrea.deflaviis@graduate.univaq.it (Andrea De Flaviis)

paper, after proper optimization and experimental validation, could help the implementation of Nonlinear Energy Sinks on real bridge decks.

Keywords:

Nonlinear energy sink, Generalized beam theory, Passive vibration control, Analytical solution

1. Introduction

Passive vibration control of civil engineering structures is a central and actual topic that involves more and more researchers. Its roots can be found in the pioneering patent of Frahm [1] which, after its publication, led to the spread of linear devices called Tuned Mass Dampers (TMD) [2–8]. The TMD is efficient at a narrow frequency width, i.e. around the tuned frequency, but it loses its efficiency elsewhere and moreover its mass can be quite big, which can result in a practical problem. Roberson [9] has been one of the first to extend the concept of passive vibrations control to nonlinear devices, using a spring with a linear and a cubic term, paving the way to other nonlinear systems. As a consequence, an evolution of those systems started in last two decades, through the use of nonlinear devices, mainly Nonlinear Energy Sinks (NES) especially with cubic nonlinearity [10–16]. Their main characteristics, that distinguish them from TMDs are the low weight with respect to the main mass and the nonlinear (and nonlinearizable) stiffness, which enables them to control a wide range of frequencies; moreover, as TMDs, they are also equipped with a damper, which enables them to dissipate the energy which is transferred in one way from the main structure to the NES [17]. In the literature, large emphasis has been given to NESs with cubic nonlinearity, but other types of devices, like non-smooth NES, vibro-impact NES, rotary NES, NES with nonlinear damping and others have been considered too [18–26]. Even if the majority of works focuses on discrete systems, significant contributions about continuous systems can also be found such as for beams and cables [27–31].

The dynamical behavior of the main structure coupled to the NES can be analytically addressed in different ways: among them, the most diffused methods are Complexification Averaging (CXA) with Multiple Scales Method (MSM) [32–34] and the Multiple Scales/Harmonic Balance Method (MSHBM) [35, 36].

In this work, the main structure to be controlled by the NES is a beam,

which is modeled through Generalized Beam Theory (GBT), an analytical formulation specifically developed to solve problems related to Thin-Walled Beams (TWB), to take into account fundamental aspects, e.g. the deformation of the cross-section in its own plane and out-of plane. The primordial idea is traced back to the work of Schardt in 1966 [37], but a great impulse was given in 90's with his contribute and that of other authors among which Davies and Leach [38–40]. Since then, works based on GBT rapidly grew up in number, facing a wide spectrum of problems. Among them those realized by Silvestre, Camotim et al. deserve a special mention: see [41–45] and related bibliography. In the meanwhile, Luongo et al. [46, 47] developed an alternative procedure to perform the first phase of GBT, namely the cross-section analysis, proposing the so called GBT-D. It has been used by the authors in [48] to compare the static and free dynamic responses of a beam modeled through GBT with the ones obtained from experimental results, showing that the model is able to capture the real beam behaviors. Moreover, in that work an Euler-Bernoulli model has been used too, highlighting that it cannot correctly predict the behavior of the box-girder beam, even for static loads.

The use of GBT in this work is motivated by the shape of the beam cross-section and by the necessity of considering different types of loads with different frequencies, which can excite certain vibration modes having torsional or local nature, that cannot be identified with simple beam theories like Euler-Bernoulli or Timoshenko ones. In addition, a classical beam theory cannot take into account the deformation of the cross-section in and out-of plane which can be a crucial aspect for some load cases.

On the other side, it is shown that using a nonlinear device like a NES for vibration control, rather than a linear one, vibrations amplitude can be effectively reduced in a wide range of frequencies, with the same NES in a very effective way.

The paper is organized as follows. In Sect. 2 the fundamental concepts of GBT are introduced with main equations, then in Sect. 3 the NES is added and the nonlinear problem is explained in detail at fast and slow time scales. In Sect. 4 different types of loads are introduced and in Sect. 5 results are reported. Conclusions and future perspectives are resumed in Sect. 6.

2. Analytical model

The system under analysis is constituted by a simply supported elastic beam having initial length L and boxed cross-section (see Fig. 1). It is representative of the generic span of a simply supported bridge, where the deformation effect of the pillars is assumed negligible and the spans are independent. The model tries to portray a real existing pre-stressed reinforced concrete beam despite some hypotheses made in the modelization and in the choice of some parameters.

A brief description of modeling according to the GBT-D technique is given here, while more details can be found in [46, 47]. The displacement field is written as a linear combination of pre-determined “deformation modes” of the cross-section, depending on its curvilinear abscissa, and unknown “amplitude functions”, depending on the axial coordinate and time. In this way a TWB can be studied in a simplified manner, without losing its typical features.

GBT is made of two main phases: (i) the cross-section analysis, which is the distinctive feature of the procedure, where the deformation modes are determined (more details can be found in Sect. 2.1) and (ii) the member-analysis, where the equilibrium equations are solved with respect to the amplitude functions, thus getting the displacement field of the beam (more details can be found in Sect. 2.2). Both of these phases are essential: the first one to correctly model the deformation of the cross-section, the second one to solve the problem, thus finding the solution. Deformation modes can be classified in accordance with GBT-D as: (i) conventional: with the Vlasov’s hypotheses of membrane inextensibility in the tangential direction and membrane shear indeformability (among these modes another subdivision can be made into rigid, distortional and local), (ii) extensional: where the hypothesis of membrane inextensibility is released and (iii) shear or warping: particularly important for short beams.

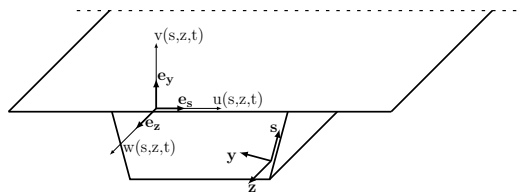


Figure 1: Cross-section with displacement field

With reference to Fig. 1, s , y and z are the tangential, transversal and ax-

ial coordinate of every element making up the section, and $u(s, z, t)$, $v(s, z, t)$ and $w(s, z, t)$ are the displacement components in the respective directions. Using the aforementioned combination of conventional deformation modes $\mathbf{U}(s)$, $\mathbf{V}(s)$ and $\mathbf{\Omega}(s)$ (the first two terms are non-dimensional, the third has dimension of a length) with amplitude functions $\boldsymbol{\varphi}(z, t)$ (with dimension of a length), the displacement field is the following (all previous are n_d column vector functions, where n_d is the number of chosen deformation modes):

$$\begin{cases} u(s, z, t) = \mathbf{U}^T(s)\boldsymbol{\varphi}(z, t) \\ v(s, z, t) = \mathbf{V}^T(s)\boldsymbol{\varphi}(z, t) \\ w(s, z, t) = \mathbf{\Omega}^T(s)\boldsymbol{\varphi}'(z, t) \end{cases} \quad (1)$$

where the first derivative on $\boldsymbol{\varphi}(z, t)$ is due to the hypothesis of membrane shear indeformability. Then, the strain field (with axial ε and shear γ strains), with membrane (superscript m) and flexural (superscript f) components, is written as:

$$\begin{pmatrix} \varepsilon_s^m \\ \varepsilon_z^m \\ \gamma_{zs}^m \\ \varepsilon_s^f \\ \varepsilon_z^f \\ \gamma_{zs}^f \end{pmatrix} = \begin{pmatrix} u_{,s} \\ w_{,z} \\ u_{,z} + w_{,s} \\ -yv_{,ss} \\ -yv_{,zz} \\ -2yv_{,sz} \end{pmatrix} = \begin{pmatrix} \mathbf{U}^T \boldsymbol{\varphi} \\ \mathbf{\Omega}^T \boldsymbol{\varphi}'' \\ (\mathbf{U}^T + \mathbf{\Omega}^T) \boldsymbol{\varphi}' \\ -y\mathbf{V}^T \boldsymbol{\varphi} \\ -y\mathbf{V}^T \boldsymbol{\varphi}'' \\ -2y\mathbf{V}^T \boldsymbol{\varphi}' \end{pmatrix} \quad (2)$$

Considering a linear elastic behavior, the active plane stress vector is written as follows, where E is Young modulus, G is shear modulus, ν is Poisson's ratio, σ and τ are the axial and shear stress respectively.

$$\begin{pmatrix} \sigma_s^m \\ \sigma_z^m \\ \tau_{zs}^m \\ \sigma_s^f \\ \sigma_z^f \\ \tau_{zs}^f \end{pmatrix} = \begin{bmatrix} E & 0 & 0 & 0 & 0 & 0 \\ 0 & E & 0 & 0 & 0 & 0 \\ 0 & 0 & G & 0 & 0 & 0 \\ 0 & 0 & 0 & \frac{E}{1-\nu^2} & \frac{\nu E}{1-\nu^2} & 0 \\ 0 & 0 & 0 & \frac{\nu E}{1-\nu^2} & \frac{E}{1-\nu^2} & 0 \\ 0 & 0 & 0 & 0 & 0 & G \end{bmatrix} \begin{pmatrix} \varepsilon_s^m \\ \varepsilon_z^m \\ \gamma_{zs}^m \\ \varepsilon_s^f \\ \varepsilon_z^f \\ \gamma_{zs}^f \end{pmatrix} \quad (3)$$

Since only conventional deformation modes are kept, $\varepsilon_s^m = 0$ and $\gamma_{zs}^m = 0$ or $\gamma_{zs}^m = \text{const}$ on closed loops. Using Hamilton's Principle, in the general

dynamical case, the following equilibrium equation with boundary conditions is obtained:

$$\begin{aligned} & \mathbf{M}\ddot{\boldsymbol{\varphi}}(z, t) - \mathbf{Q}_{\Omega\Omega}^M \ddot{\boldsymbol{\varphi}}''(z, t) + (\mathbf{C}^f + \mathbf{C}_{\Omega\Omega}^a) \boldsymbol{\varphi}''''(z, t) \\ & + (\mathbf{D}^f + \mathbf{D}^{fT} - \mathbf{D}_{\Omega\Omega}^s - \mathbf{D}^t) \boldsymbol{\varphi}''(z, t) + \mathbf{B}^f \boldsymbol{\varphi}(z, t) \\ & = \mathbf{p}_{\Omega}(z, t) \end{aligned} \quad (4)$$

$$\delta \boldsymbol{\varphi}^{iT}(z, t) [(\mathbf{C}^f + \mathbf{C}_{\Omega\Omega}^a) \boldsymbol{\varphi}''(z, t) + \mathbf{D}^f \boldsymbol{\varphi}(z, t)]|_0^L = 0 \quad \forall t \quad (5)$$

$$\begin{aligned} & \delta \boldsymbol{\varphi}^T(z, t) [-\mathbf{Q}_{\Omega\Omega}^M \ddot{\boldsymbol{\varphi}}'(z, t) + (\mathbf{C}^f + \mathbf{C}_{\Omega\Omega}^a) \boldsymbol{\varphi}'''(z, t) \\ & + (\mathbf{D}^f - \mathbf{D}_{\Omega\Omega}^s - \mathbf{D}^t) \boldsymbol{\varphi}'(z, t)]|_0^L = 0 \quad \forall t \end{aligned} \quad (6)$$

The symmetric n_d mass and stiffness matrices (\mathbf{M} , $\mathbf{Q}_{\Omega\Omega}^M$, \mathbf{C}^f , ...) written in Eqs. (4-6) are the following, where m is mass per unit area and h is thickness along y . Moreover, \mathbf{p}_{Ω} is the load vector in the general case of forces per unit area applied in all three directions:

$$\mathbf{M} = \int_s m(\mathbf{U}\mathbf{U}^T + \mathbf{V}\mathbf{V}^T) ds, \quad \mathbf{Q}_{\Omega\Omega}^M = \int_s m\boldsymbol{\Omega}\boldsymbol{\Omega}^T ds \quad (7)$$

$$\mathbf{C}^f = \int_s \frac{Eh^3}{12(1-\nu^2)} \mathbf{V}\mathbf{V}^T ds, \quad \mathbf{C}_{\Omega\Omega}^a = \int_s Eh\boldsymbol{\Omega}\boldsymbol{\Omega}^T ds \quad (8)$$

$$\mathbf{D}_{\Omega\Omega}^s = \int_s Gh(\boldsymbol{\Omega}^{iT} + \mathbf{U}^T)^T (\boldsymbol{\Omega}^{iT} + \mathbf{U}^T) ds \quad (9)$$

$$\mathbf{D}^f = \int_s \frac{\nu Eh^3}{12(1-\nu^2)} \mathbf{V}\mathbf{V}''^T ds, \quad \mathbf{D}^t = \int_s \frac{Gh^3}{3} \mathbf{V}'\mathbf{V}'^T ds \quad (10)$$

$$\mathbf{B}^f = \int_s \frac{Eh^3}{12(1-\nu^2)} \mathbf{V}''\mathbf{V}''^T ds \quad (11)$$

$$\mathbf{p}_{\Omega} = \int_s (f_s \mathbf{U} + f_y \mathbf{V} - f'_z \boldsymbol{\Omega}) ds \quad (12)$$

2.1. Cross-section analysis

Cross-section analysis is a crucial step of GBT, as it involves the determination of deformation modes of the cross-section which affects the quality of the response. A full detailed explanation of how it is performed in the framework of GBT-D can be found in [47]; main features are here resumed. Basically, to find conventional modes, the free dynamics problem of the externally unrestrained cross-section (in the plane orthogonal to z) has to be studied, which implies, in the order, the following steps:

- (i) The cross-section is discretized in finite elements (FE) by introducing intermediate nodes, each of which has 3 degrees of freedom (two translations and one rotation). The classical stiffness and mass matrices of each element are built and then assembled to get those of the entire cross-section.
- (ii) The internal restraint of membrane inextensibility is applied and the dynamical eigenvalue problem with reduced matrices is solved. Since no external restraint exists, 3 zero eigenvalues are found and the corresponding eigenvectors (nodal dofs) represent rigid modes (two translation and one rotation in the plane). The tangential and transversal components of deformation modes $\mathbf{U}(s)$ and $\mathbf{V}(s)$ are obtained from nodal displacements through linear and cubic interpolation functions, respectively.
- (iii) Making use of membrane shear indeformability hypothesis, the longitudinal components of deformation modes $\mathbf{\Omega}(s)$ are also found, directly related to $\mathbf{U}(s)$. To get the complete set of conventional deformation modes, a fourth rigid mode, representing translation along z , has to be added (this is normally obtained as the first of shear or warping modes, not considered in this work).

Some of cross-section deformation modes are shown in Fig. 2 in terms of displacements in the plane of the cross-section (labeled as $\mathbf{U}(s)$, $\mathbf{V}(s)$) and along the beam axis (labeled as $\mathbf{\Omega}(s)$).

2.2. Member analysis

Member analysis, i.e. resolution of equilibrium Eqs. (4-6) to find the unknowns $\boldsymbol{\varphi}(z, t)$ can be performed either analytically or numerically, e.g. using finite elements for the latter. In the case of a simply supported beam,

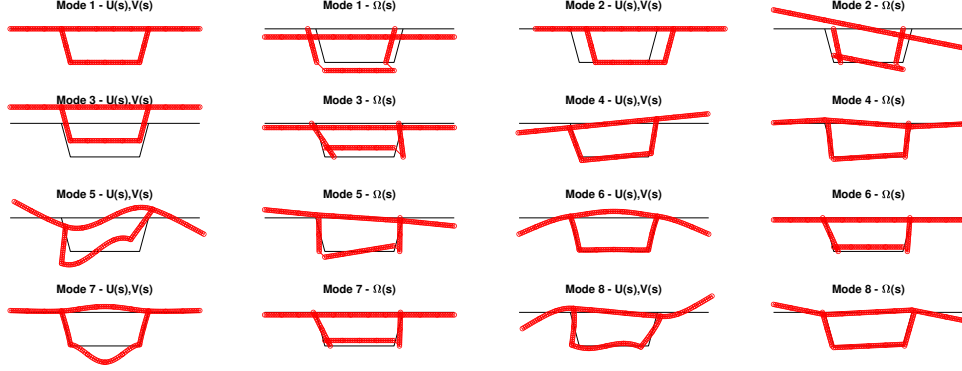


Figure 2: First conventional deformation modes with in-plane and out-of plane components

as in the present work, it has been shown in [49] that an analytical solution is possible, both for free and forced dynamics. The analytical solution in free dynamics, i.e. natural frequencies and vibration modes, is here resumed, since it will be used in the following. Considering the j^{th} vibration mode, free dynamics equation with boundary conditions representing simply supported beam, derived from Eqs. (4-6), are:

$$\begin{aligned} \mathbf{M}\ddot{\boldsymbol{\varphi}}_j(z, t) - \mathbf{Q}_{\Omega\Omega}^M \ddot{\boldsymbol{\varphi}}_j''(z, t) + (\mathbf{C}^f + \mathbf{C}_{\Omega\Omega}^a) \boldsymbol{\varphi}_j''''(z, t) \\ + (\mathbf{D}^f + \mathbf{D}^{fT} - \mathbf{D}_{\Omega\Omega}^s - \mathbf{D}^t) \boldsymbol{\varphi}_j''(z, t) + \mathbf{B}^f \boldsymbol{\varphi}_j(z, t) = \mathbf{0} \end{aligned} \quad (13)$$

$$[(\mathbf{C}^f + \mathbf{C}_{\Omega\Omega}^a) \boldsymbol{\varphi}_j''(z, t) + \mathbf{D}^f \boldsymbol{\varphi}_j(z, t)]|_0^L = \mathbf{0} \quad \forall t \quad (14)$$

$$\boldsymbol{\varphi}_j(z, t)|_0^L = \mathbf{0} \quad \forall t \quad (15)$$

where the j^{th} amplitude function can be written separating space and time as:

$$\boldsymbol{\varphi}_j(z, t) = \boldsymbol{\Phi}_j(z) Y_j(t) \quad (16)$$

where $\boldsymbol{\Phi}_j(z)$ is the column vector of dimension n_d representing the j^{th} vibration mode, while $Y_j(t)$ is the modal coordinate. As a consequence, Eq. (13)

can be split into the following (ω_j being the j^{th} angular frequency in rad/s):

$$\ddot{Y}_j(t) + \omega_j^2 Y_j(t) = 0 \quad (17)$$

$$\begin{aligned} & (\mathbf{C}^f + \mathbf{C}_{\Omega\Omega}^a) \Phi_j''''(z) + (\mathbf{D}^f + \mathbf{D}^{fT} - \mathbf{D}_{\Omega\Omega}^s - \mathbf{D}^t) \Phi_j''(z) \\ & + \mathbf{B}^f \Phi_j(z) - \omega_j^2 (\mathbf{M} \Phi_j(z) - \mathbf{Q}_{\Omega\Omega}^M \Phi_j''(z)) = \mathbf{0} \end{aligned} \quad (18)$$

The goal is to analytically solve Eq. (18) to find natural frequencies and vibration modes. To do that, it can be observed that a solution that satisfies boundary conditions (5),(6) is:

$$\Phi_j(z) = \Theta_j \sin\left(\frac{n_j \pi z}{L}\right) \quad (19)$$

where Θ_j and n_j are the magnitude and the longitudinal half-wave number of the j^{th} vibration mode, respectively. The magnitudes, as well as the squared angular frequencies ω_j^2 , are determined substituting Eq. (19) into Eq. (18), thus obtaining a problem like:

$$(\mathbf{K}_j - \omega_j^2 \mathbf{M}_j) \Theta_j = \mathbf{0} \quad (20)$$

where the stiffness and mass matrices are:

$$\mathbf{K}_j = (\mathbf{C}^f + \mathbf{C}_{\Omega\Omega}^a) \left(\frac{n_j \pi}{L}\right)^4 - (\mathbf{D}^f + \mathbf{D}^{fT} - \mathbf{D}_{\Omega\Omega}^s - \mathbf{D}^t) \left(\frac{n_j \pi}{L}\right)^2 + \mathbf{B}^f \quad (21)$$

$$\mathbf{M}_j = \mathbf{M} + \mathbf{Q}_{\Omega\Omega}^M \left(\frac{n_j \pi}{L}\right)^2 \quad (22)$$

Solving the eigenvalue problem (20), the total number of vibration modes is $n_v = n_d \times N_j$ with N_j maximum half-wave number considered; some of them are showed in Fig. 3.

It can be proved, following classical steps (projection on a generic vibration mode $\Phi_h(z)$), that orthogonality with respect to the mass and stiffness operators exists among all found vibration modes. This means that, in the generic case where a dynamical force acts on the beam, uncoupled equations can be solved for every vibration mode and their contribution summed, retaining only a limited number of modes:

$$\varphi(z, t) = \sum_{j=1}^{n_v} \Phi_j(z) Y_j(t) = \Phi(z) \mathbf{Y}(t) \quad (23)$$

where $\Phi(z)$ is a $n_d \times n_v$ matrix function where each row corresponds to a deformation mode and each column to a vibration mode, while $\mathbf{Y}(t)$ is a n_v column vector function, where each row is the time response of a vibration mode to a given load. As a consequence, substituting Eq. (23) inside Eq. (1), the transversal displacement becomes:

$$v(s, z, t) = \mathbf{V}^T(s) \Phi(z) \mathbf{Y}(t)$$

$$= (V_1(s) \ \dots \ V_{n_d}(s)) \begin{bmatrix} \Phi_{11}(z) & \dots & \Phi_{1n_v}(z) \\ \vdots & \ddots & \vdots \\ \Phi_{n_d1}(z) & \dots & \Phi_{n_d n_v}(z) \end{bmatrix} \begin{pmatrix} Y_1(t) \\ \vdots \\ Y_{n_v}(t) \end{pmatrix} \quad (24)$$

This representation emphasizes the difference between deformation modes and vibration modes and highlights the possibility to choose an arbitrary number of each of them.

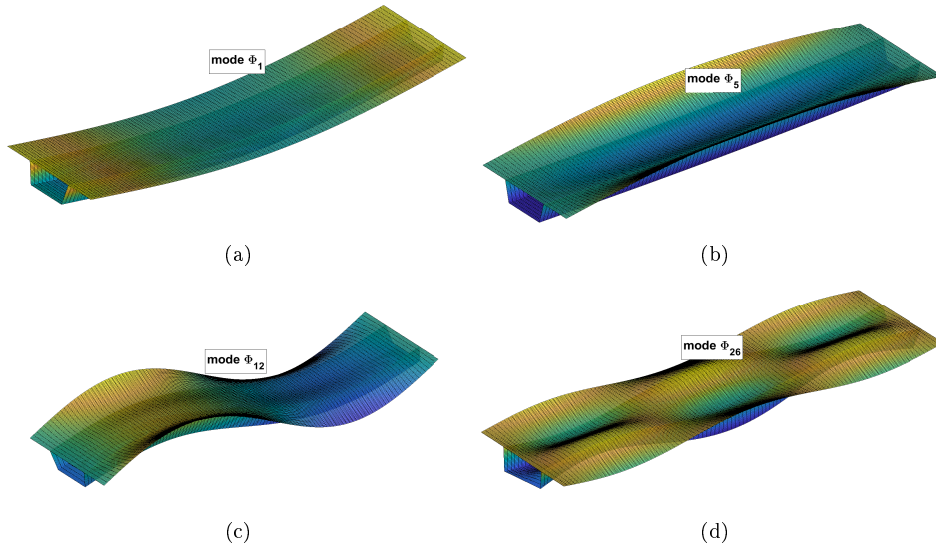


Figure 3: Some of the n_v vibration modes. (a) $n_j = 1$: Φ_1 , (b) $n_j = 1$: Φ_5 ; (c) $n_j = 2$: Φ_{12} ; (d) $n_j = 3$: Φ_{26}

3. Nonlinear problem

In this Section, a NES is added to the beam, with the objective of controlling vibrations due to different types of loads.

3.1. Formulation

The NES is shown in Fig. 4 together with a sketch of the simply supported beam representing the longitudinal direction of the bridge, where m_N , k_N and c_N are the mass, cubic stiffness and damping of the NES respectively, z_N being its position along the beam axis and $y_N(t)$ its absolute vertical displacement.

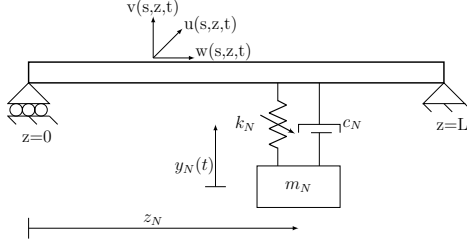


Figure 4: Scheme of the beam coupled with NES

Equilibrium equations of the undamped beam with the attached NES can be written as follows, where all symbols have been explained before:

$$\begin{aligned}
\mathbf{M}\ddot{\boldsymbol{\varphi}}(z, t) - \mathbf{Q}_{\Omega\Omega}^M \ddot{\boldsymbol{\varphi}}''(z, t) + (\mathbf{C}^f + \mathbf{C}_{\Omega\Omega}^a) \boldsymbol{\varphi}''''(z, t) \\
+ (\mathbf{D}^f + \mathbf{D}^{fT} - \mathbf{D}_{\Omega\Omega}^s - \mathbf{D}^t) \boldsymbol{\varphi}''(z, t) + \mathbf{B}^f \boldsymbol{\varphi}(z, t) \\
+ \mathbf{V}(s_N) [k_N (\mathbf{V}^T(s_N) \boldsymbol{\varphi}(z, t) - y_N(t))^3 \\
+ c_N (\mathbf{V}^T(s_N) \dot{\boldsymbol{\varphi}}(z, t) - \dot{y}_N(t))] \delta(z - z_N) = \mathbf{p}_\Omega(z, t)
\end{aligned} \tag{25}$$

$$\begin{aligned}
m_N \ddot{y}_N(t) - [k_N (\mathbf{V}^T(s_N) \boldsymbol{\varphi}(z_N, t) - y_N(t))^3 \\
+ c_N (\mathbf{V}^T(s_N) \dot{\boldsymbol{\varphi}}(z_N, t) - \dot{y}_N(t))] = 0
\end{aligned} \tag{26}$$

$\delta(z - z_N)$ is the Dirac function, which provides the position of the NES along the beam. Since the goal is to study a 1:1 resonance and internal resonances are not considered, it can be assumed that the response of the system is dominated by its j^{th} vibration mode, i.e. $\boldsymbol{\varphi}(z, t) = \boldsymbol{\Phi}_j(z) Y_j(t)$ and Eq. (25) is projected on it. Furthermore, at this point damping is added to the beam as $C_j = 2\xi_j M_j \omega_j$ where ξ_j is modal damping coefficient.

$$\begin{aligned}
M_j \ddot{Y}_j(t) + C_j \dot{Y}_j(t) + K_j Y_j(t) \\
+ \boldsymbol{\Phi}_j^T(z_N) \mathbf{V}(s_N) [k_N (\mathbf{V}^T(s_N) \boldsymbol{\Phi}_j(z_N) Y_j(t) - y_N(t))^3 \\
+ c_N (\mathbf{V}^T(s_N) \boldsymbol{\Phi}_j(z_N) \dot{Y}_j(t) - \dot{y}_N(t))] = \int_0^L \boldsymbol{\Phi}_j^T(z) \mathbf{p}_\Omega(z, t) dz
\end{aligned} \tag{27}$$

$$\begin{aligned}
& m_N \ddot{y}_N(t) - [k_N(\mathbf{V}^T(s_N)\boldsymbol{\Phi}_j(z_N)Y_j(t) - y_N(t))^3 \\
& + c_N(\mathbf{V}^T(s_N)\boldsymbol{\Phi}_j(z_N)\dot{Y}_j(t) - \dot{y}_N(t))] = 0
\end{aligned} \tag{28}$$

where mass and stiffness terms are:

$$M_j = \int_0^L \boldsymbol{\Phi}_j^T(z) [\mathbf{M}\boldsymbol{\Phi}_j(z) - \mathbf{Q}_{\Omega\Omega}^M \boldsymbol{\Phi}_j''(z)] dz \tag{29}$$

$$\begin{aligned}
K_j &= \int_0^L \boldsymbol{\Phi}_j^T(z) [(\mathbf{C}^f + \mathbf{C}_{\Omega\Omega}^a) \boldsymbol{\Phi}_j''''(z) \\
&+ (\mathbf{D}^f + \mathbf{D}^{fT} - \mathbf{D}_{\Omega\Omega}^s - \mathbf{D}^t) \boldsymbol{\Phi}_j''(z) + \mathbf{B}^f \boldsymbol{\Phi}_j(z)] dz
\end{aligned} \tag{30}$$

Non-dimensional parameters are introduced as follows:

$$\tilde{z} = \frac{z}{b_1}, \quad \tau = \omega_j t, \quad \tilde{y}_N(\tau) = \frac{y_N(t)}{b_1} \tag{31}$$

$$\varepsilon \tilde{k}_N = \frac{k_N b_1^2}{K_j}, \quad \varepsilon \tilde{c}_N = \frac{c_N \omega_j}{K_j}, \quad \varepsilon \hat{C}_j = 2\xi_j \tag{32}$$

$$\tilde{\mathbf{V}}(\tilde{s}_N) = \mathbf{V}(s_N), \quad \tilde{\boldsymbol{\Phi}}_j(\tilde{z}_N) = \boldsymbol{\Phi}_j(z_N), \quad \tilde{Y}_j(\tau) = \frac{Y_j(t)}{b_1} \tag{33}$$

$$\varepsilon \Gamma = \frac{1}{M_j \omega_j^2 b_1} \int_0^L \boldsymbol{\Phi}_j^T(z) \mathbf{p}_\Omega(z, t) dz \tag{34}$$

where b_1 is a characteristic length of the beam and ε is a small non-dimensional parameter accounting for the ratio between the mass of the NES and that of the beam to be controlled as:

$$0 < \varepsilon = \frac{m_N}{M_j} \ll 1 \tag{35}$$

Putting non-dimensional variables into Eqs. (27-28), they become the following, where $\dot{(\cdot)} = d/d\tau$:

$$\begin{aligned}
& \ddot{\tilde{Y}}_j(\tau) + \varepsilon \hat{C}_j \dot{\tilde{Y}}_j(\tau) + \tilde{Y}_j(\tau) \\
& + \tilde{\boldsymbol{\Phi}}_j^T(\tilde{z}_N) \tilde{\mathbf{V}}(\tilde{s}_N) [\varepsilon \tilde{k}_N (\tilde{\mathbf{V}}^T(\tilde{s}_N) \tilde{\boldsymbol{\Phi}}_j(\tilde{z}_N) \tilde{Y}_j(\tau) - \tilde{y}_N(\tau))^3 \\
& + \varepsilon \tilde{c}_N (\tilde{\mathbf{V}}^T(\tilde{s}_N) \tilde{\boldsymbol{\Phi}}_j(\tilde{z}_N) \dot{\tilde{Y}}_j(\tau) - \dot{\tilde{y}}_N(\tau))] = \varepsilon \Gamma
\end{aligned} \tag{36}$$

$$\begin{aligned} \varepsilon \ddot{y}_N(\tau) - [\varepsilon \tilde{k}_N (\tilde{\mathbf{V}}^T(\tilde{s}_N) \tilde{\Phi}_j(\tilde{z}_N) \dot{Y}_j(\tau) - \dot{y}_N(\tau))]^3 \\ + \varepsilon \tilde{c}_N (\tilde{\mathbf{V}}^T(\tilde{s}_N) \tilde{\Phi}_j(\tilde{z}_N) \dot{Y}_j(\tau) - \dot{y}_N(\tau))] = 0 \end{aligned} \quad (37)$$

Equations are rearranged introducing new variables representing the relative displacement a between the beam and the NES, in the point where the NES is attached, and a quantity r which represents the displacement of the center of mass of the coupled system as:

$$\begin{pmatrix} a \\ r \end{pmatrix} = \begin{bmatrix} \tilde{\mathbf{V}}^T(\tilde{s}_N) \tilde{\Phi}_j(\tilde{z}_N) & -1 \\ 1 & \varepsilon \end{bmatrix} \begin{pmatrix} \tilde{Y}_j \\ \tilde{y}_N \end{pmatrix} \quad (38)$$

So, equilibrium equations are rewritten, with $\chi_j = \tilde{\Phi}_j^T(\tilde{z}_N) \tilde{\mathbf{V}}(\tilde{s}_N)$ and $D = 1 + \varepsilon \chi_j$, as:

$$\begin{aligned} \ddot{r} + \frac{\varepsilon \hat{C}_j}{D} (\varepsilon \dot{a} + \dot{r}) + \frac{1}{D} (\varepsilon a + r) + \varepsilon \tilde{k}_N (\chi_j - 1) a^3 \\ + \varepsilon \tilde{c}_N (\chi_j - 1) \dot{a} = \varepsilon \Gamma \end{aligned} \quad (39)$$

$$\begin{aligned} \ddot{a} + \frac{\varepsilon \chi_j \hat{C}_j}{D} (\varepsilon \dot{a} + \dot{r}) + \frac{\chi_j}{D} (\varepsilon a + r) + \tilde{k}_N (\varepsilon \chi_j^2 + 1) a^3 \\ + \tilde{c}_N (\varepsilon \chi_j^2 + 1) \dot{a} = \varepsilon \chi_j \Gamma \end{aligned} \quad (40)$$

In the spirit of the Complexification Averaging Method, complex variables β_1, β_2 by Manevitch [32] are introduced (i is the imaginary unit):

$$\begin{cases} \beta_1 e^{i\Omega\tau} = \dot{r} + i\Omega r \\ \beta_2 e^{i\Omega\tau} = \dot{a} + i\Omega a \end{cases} \quad (41)$$

At this point, since the goal is to solve the problem through Multiple Scales Method [33], different time scales are introduced and complex variables are rewritten as:

$$\beta_j(\tau) = \beta_j(\tau_0, \tau_1, \dots), \quad \tau_i = \varepsilon^i \tau, \quad i = 1, 2 \quad (42)$$

and applying Galerkin's method, using $()^*$ to denote complex conjugate of a variable, only harmonic of frequency Ω is kept, i.e.:

$$x(\beta_1, \beta_2, \beta_1^*, \beta_2^*) = \frac{\Omega}{2\pi} \int_0^{2\pi} X(\beta_1, \beta_2, \beta_1^*, \beta_2^*) e^{-i\Omega\tau} d\tau \quad (43)$$

The hypothesis, to be proved, is that variables β_j do not depend on the fast time scale $\tau_0 = \tau$ (or system will be studied at the infinity of fast time scale, i.e. for $\tau_0 \rightarrow \infty$). As a consequence, equilibrium equations are finally rewritten as:

$$\begin{aligned}
& \dot{\beta}_1 + \frac{i\Omega}{2}\beta_1 + \frac{\varepsilon\hat{C}_j}{2D}(\beta_1 + \varepsilon\beta_2) + \frac{1}{2i\Omega D}(\beta_1 + \varepsilon\beta_2) \\
& + \frac{3}{8i\Omega^3}\varepsilon\tilde{k}_N(\chi_j - 1)\beta_2^2\beta_2^* + \frac{1}{2}\varepsilon\tilde{c}_N(\chi_j - 1)\beta_2 \\
& = \frac{\Omega}{2\pi} \int_0^{2\pi} \frac{\Omega}{\Omega} \varepsilon\Gamma e^{-i\Omega\tau} d\tau
\end{aligned} \tag{44}$$

$$\begin{aligned}
& \dot{\beta}_2 + \frac{i\Omega}{2}\beta_2 + \frac{\varepsilon\chi_j\hat{C}_j}{2D}(\beta_1 + \varepsilon\beta_2) + \frac{\chi_j}{2i\Omega D}(\beta_1 + \varepsilon\beta_2) \\
& + \frac{3}{8i\Omega^3}\tilde{k}_N(\varepsilon\chi_j^2 + 1)\beta_2^2\beta_2^* + \frac{1}{2}\tilde{c}_N(\varepsilon\chi_j^2 + 1)\beta_2 \\
& = \frac{\Omega}{2\pi} \int_0^{2\pi} \frac{\Omega}{\Omega} \varepsilon\chi_j\Gamma e^{-i\Omega\tau} d\tau
\end{aligned} \tag{45}$$

where the derivative with respect to non-dimensional time is:

$$\frac{d(\dots)}{d\tau} = \frac{\partial(\dots)}{\partial\tau_0} + \varepsilon\frac{\partial(\dots)}{\partial\tau_1} + \varepsilon^2\frac{\partial(\dots)}{\partial\tau_2} + \dots = d_0 + \varepsilon d_1 + \varepsilon^2 d_2 + \dots \tag{46}$$

As a consequence of the introduction of multiple scales, the system behavior is studied at different orders of ε , i.e. at different scales of time, with the higher orders ε being corrections to the lower order ones. Moreover, to study the system around a 1:1 resonance, it should be set:

$$\Omega = \Omega_F/\omega_j = 1 + \varepsilon\sigma \tag{47}$$

where Ω_F is the angular frequency of the external load and σ is a detuning parameter that permits to study the system near the resonance. Collecting all terms at the same order of ε until ε^1 leads to:

$$\text{order } \varepsilon^0 : d_0\beta_1 + \frac{i}{2}\beta_1 + \frac{1}{2iD}\beta_1 = 0 \tag{48}$$

$$d_0\beta_2 + \frac{i}{2}\beta_2 + \frac{\chi_j}{2iD}\beta_1 + \frac{3}{8i}\tilde{k}_N\beta_2^2\beta_2^* + \frac{1}{2}\tilde{c}_N\beta_2 = 0 \quad (49)$$

$$\begin{aligned} \text{order } \varepsilon^1 : d_1\beta_1 + \frac{i\sigma}{2}\beta_1 + \frac{\hat{C}_j}{2D}\beta_1 + \frac{1}{2iD}(\beta_2 - \sigma\beta_1) \\ + \frac{3}{8i}\tilde{k}_N(\chi_j - 1)\beta_2^2\beta_2^* + \frac{1}{2}\tilde{c}_N(\chi_j - 1)\beta_2 = \frac{\Omega}{2\pi} \int_0^{2\pi} \Gamma e^{-i\Omega\tau} d\tau \end{aligned} \quad (50)$$

$$\begin{aligned} d_1\beta_2 + \frac{i\sigma}{2}\beta_2 + \frac{\chi_j\hat{C}_j}{2D}\beta_1 + \frac{\chi_j}{2iD}(\beta_2 - \sigma\beta_1) \\ + \frac{3}{8i}\tilde{k}_N(\chi_j^2 - 3\sigma)\beta_2^2\beta_2^* + \frac{1}{2}\tilde{c}_N\chi_j^2\beta_2 = \frac{\Omega}{2\pi} \int_0^{2\pi} \chi_j \Gamma e^{-i\Omega\tau} d\tau \end{aligned} \quad (51)$$

3.2. Fast time scale

Starting from Eq. (48), since $D \approx 1$, it results that $d_0\beta_1 = 0$, which means that β_1 is independent of fast time τ_0 in accordance to the hypothesis made before. About Eq. (49), an asymptotic state is searched for $\tau_0 \rightarrow \infty$, so that $d_0\beta_2 = 0$: this means finding the equilibrium (fixed) points of the system. Doing that, the following equation is obtained:

$$\mathbb{S}(\beta_1, \beta_2, \beta_1^*, \beta_2^*) = \frac{\chi_j}{2i}\beta_1 - \frac{1}{2i}\beta_2 + \frac{3}{8i}\tilde{k}_N\beta_2^2\beta_2^* + \frac{1}{2}\tilde{c}_N\beta_2 = 0 \quad (52)$$

This is the equation of the Slow Invariant Manifold (SIM), a topological manifold, invariant under the action of a dynamical system [50, 51]. To study it, complex variables are written in polar form as:

$$\beta_j = N_j e^{i\delta_j}, \quad j = 1, 2 \quad (53)$$

where $N_j \in \mathbb{R}^+$, $\delta_j \in \mathbb{R}$. Putting Eq. (53) into Eq. (52), the SIM in the real domain is obtained, thus finding the searched equilibrium points:

$$N_1 = \frac{N_2}{\chi_j} \sqrt{\tilde{c}_N^2 + \left(1 - \frac{3}{4}\tilde{k}_N N_2^2\right)^2} \quad (54)$$

To trace stable and unstable zones of the SIM, a small linear perturbation $|\Delta\beta_2| \ll |\beta_2|$ is applied to β_2 , i.e. $\beta_2 \rightarrow \beta_2 + \Delta\beta_2$ and the same to its complex conjugate. The real part of the eigenvalues of the resulting matrix is studied: if it is negative, the equilibrium points are classified as stable, otherwise they are unstable. After neglecting higher order terms, equation becomes:

$$\begin{pmatrix} \frac{\delta\Delta\beta_2}{\delta\tau_0} \\ \frac{\delta\Delta\beta_2^*}{\delta\tau_0} \end{pmatrix} = \mathbf{A} \begin{pmatrix} \Delta\beta_2 \\ \Delta\beta_2^* \end{pmatrix} \quad (55)$$

where the matrix \mathbf{A} is:

$$\mathbf{A} = \begin{bmatrix} \frac{1}{2i} - \frac{3}{4i}\tilde{k}_N\beta_2\beta_2^* - \frac{1}{2}\tilde{c}_N & -\frac{3}{8i}\tilde{k}_N\beta_2^2 \\ \frac{3}{8i}\tilde{k}_N\beta_2^{*2} & -\frac{1}{2i} + \frac{3}{4i}\tilde{k}_N\beta_2\beta_2^* - \frac{1}{2}\tilde{c}_N \end{bmatrix} \quad (56)$$

The eigenvalues of \mathbf{A} verify the following characteristic polynomial:

$$\lambda^2 - (A_{11} + A_{22})\lambda + A_{11}A_{22} - A_{12}A_{21} = 0 \quad (57)$$

It can be observed that following relations exist:

$$\begin{cases} \lambda_1 + \lambda_2 = A_{11} + A_{22} = -\tilde{c}_N < 0 \\ \lambda_1\lambda_2 = A_{11}A_{22} - A_{12}A_{21} \end{cases} \quad (58)$$

This means that, since the sum between the real part of eigenvalues is always negative (being the damping coefficient of the NES positive), if the product between them is positive, both of them have to be negative, so the equilibrium point is stable, while if the product is negative, the real part of one eigenvalue is necessarily positive, so the equilibrium point is unstable. It is concluded that the unstable zones of the SIM are those for which $A_{11}A_{22} - A_{12}A_{21} < 0$.

3.3. Slow time scale

Here the goal is to study the evolution of the SIM at the slow time scale τ_1 and to study the system at slow time scale around the SIM [13], to investigate its behavior near resonance. In order to do that, equilibrium and singular points have to be found starting from the first equilibrium equation at order ε^1 , Eq. (50), written as:

$$\frac{\partial\beta_1}{\partial\tau_1} = \mathbb{E}_1(\beta_1, \beta_2, \beta_1^*, \beta_2^*) \quad (59)$$

where:

$$\begin{aligned} \mathbb{E}_1(\beta_1, \beta_2, \beta_1^*, \beta_2^*) &= \frac{\sigma}{2i}\beta_1 - \frac{\hat{C}_j}{2D}\beta_1 - \frac{1}{2i}(\beta_2 - \sigma\beta_1) \\ &- \frac{3}{8i}\tilde{k}_N(\chi_j - 1)\beta_2^2\beta_2^* - \frac{1}{2}\tilde{c}_N(\chi_j - 1)\beta_2 + \frac{\Omega}{2\pi} \int_0^{2\pi} \frac{\Omega}{\Omega} \Gamma e^{-i\Omega\tau} d\tau \end{aligned} \quad (60)$$

Moreover, the evolution of the SIM \mathbb{S} at the current time scale τ_1 has to be considered as:

$$\begin{cases} \frac{\partial \mathbb{S}}{\partial \tau_1} = \frac{\partial \mathbb{S}}{\partial \beta_1} \frac{\partial \beta_1}{\partial \tau_1} + \frac{\partial \mathbb{S}}{\partial \beta_2} \frac{\partial \beta_2}{\partial \tau_1} + \frac{\partial \mathbb{S}}{\partial \beta_1^*} \frac{\partial \beta_1^*}{\partial \tau_1} + \frac{\partial \mathbb{S}}{\partial \beta_2^*} \frac{\partial \beta_2^*}{\partial \tau_1} = 0 \\ \frac{\partial \mathbb{S}^*}{\partial \tau_1} = \frac{\partial \mathbb{S}^*}{\partial \beta_1} \frac{\partial \beta_1}{\partial \tau_1} + \frac{\partial \mathbb{S}^*}{\partial \beta_2} \frac{\partial \beta_2}{\partial \tau_1} + \frac{\partial \mathbb{S}^*}{\partial \beta_1^*} \frac{\partial \beta_1^*}{\partial \tau_1} + \frac{\partial \mathbb{S}^*}{\partial \beta_2^*} \frac{\partial \beta_2^*}{\partial \tau_1} = 0 \end{cases} \quad (61)$$

This system of equations can be reorganized in matrix form as:

$$\underbrace{\begin{bmatrix} \frac{\partial \mathbb{S}}{\partial \beta_2} & \frac{\partial \mathbb{S}}{\partial \beta_2^*} \\ \frac{\partial \mathbb{S}^*}{\partial \beta_2} & \frac{\partial \mathbb{S}^*}{\partial \beta_2^*} \end{bmatrix}}_{\mathbf{J}_2} \begin{pmatrix} \frac{\partial \beta_2}{\partial \tau_1} \\ \frac{\partial \beta_2^*}{\partial \tau_1} \end{pmatrix} = - \begin{bmatrix} \frac{\partial \mathbb{S}}{\partial \beta_1} & \frac{\partial \mathbb{S}}{\partial \beta_1^*} \\ \frac{\partial \mathbb{S}^*}{\partial \beta_1} & \frac{\partial \mathbb{S}^*}{\partial \beta_1^*} \end{bmatrix} \begin{pmatrix} \frac{\partial \beta_1}{\partial \tau_1} \\ \frac{\partial \beta_1^*}{\partial \tau_1} \end{pmatrix} \quad (62)$$

By calling \mathbf{J}_2 the Jacobian matrix of the SIM with respect to (β_2, β_2^*) the following systems can be written, for equilibrium and singular points respectively:

$$\begin{cases} \mathbb{E}_1 = 0 \\ \mathbb{S} = 0 \\ \det(\mathbf{J}_2) \neq 0 \end{cases} \quad \begin{cases} \mathbb{E}_1 = 0 \\ \mathbb{S} = 0 \\ \det(\mathbf{J}_2) = 0 \end{cases} \quad (63)$$

Computing matrix \mathbf{J}_2 , it turns out that $\mathbf{J}_2 = -\mathbf{A}$, which involves that singular points of the system are located in correspondence of the stability borders.

Equilibrium points are found investigating the first two equations of the first system in Eq. (63), namely Eq. (60) and Eq. (52), to get an equation containing N_2 , having as unknown the detuning parameter σ , such that a simple second order algebraic equation has to be solved for different values of N_2 . Setting $F = 3/4\tilde{k}_N\beta_2\beta_2^*$ and $\hat{\gamma} = \Omega/(2\pi) \int_0^{2\pi/\Omega} \Gamma e^{-i\Omega\tau} d\tau$, the first two equations of the system give:

$$c_1\sigma^2 + c_2\sigma + c_3 = 0 \quad (64)$$

where:

$$c_1 = N_2^2 \left[\left(\frac{1}{\chi_j} - \frac{F}{\chi_j} \right)^2 + \frac{\tilde{c}_N^2}{\chi_j^2} \right] \quad (65)$$

$$c_2 = N_2^2 \left(\frac{F^2(\chi_j - 1)}{\chi_j} - \frac{F(\chi_j - 1)}{\chi_j} + \frac{F}{\chi_j} - \frac{1}{\chi_j} + \frac{\tilde{c}_N^2(\chi_j - 1)}{\chi_j} \right) \quad (66)$$

$$c_3 = N_2^2 \left(\frac{F^2(\chi_j - 1)^2}{4} + \frac{F(\chi_j - 1)}{2} + \frac{\tilde{c}_N^2(\chi_j - 1)^2}{4} + \frac{1}{4} \right. \\ \left. + \frac{\hat{C}_j^2 F^2}{4\chi_j^2} - \frac{\hat{C}_j^2 F}{2\chi_j^2} + \frac{\hat{C}_j \tilde{c}_N}{2} + \frac{\hat{C}_j^2}{4\chi_j^2} + \frac{\hat{C}_j^2 \tilde{c}_N^2}{4\chi_j^2} \right) - \left| \frac{-\hat{\gamma}}{i} \right|^2 \quad (67)$$

Resolution of Eq. (64) gives maximum two values of σ for every assigned N_2 , where only real values of σ have a physical meaning. Moreover, the relationship between N_1 and σ can be obtained through Eq. (52), thus getting the frequency response curves, i.e. the relationships between the amplitudes of response N_1 and N_2 and the frequency, here represented by the detuning parameter σ . From these curves, different types of responses can be obtained as function of σ :

- (i) Periodic Response: for stable equilibrium points, with the system oscillating in time with a certain period, asymptotically tending to equilibrium.
- (ii) Modulated Response: generally speaking this response can be detected if the system presents fold singularities, i.e. when equilibrium points (obtained from $\mathbb{E}_1 = 0$ around the SIM) and singular points (for which $\det(\mathbf{J}_2) = 0$) coincide (see Eq. (63)) [12, 13, 19]. Moreover, if the equilibrium point is positioned in the unstable zone of the SIM, the system will also present the modulated response, corresponding to repeated jumps between the limit points of the SIM [22]. Physically speaking, this response is similar to beating.
- (iii) Isola: the system can present isolas as well. This isolated branch of the frequency response curve can appear for some ranges of amplitude of the external excitation and out of them it reintegrates to the main branch. It can be seen that the frequency response curve in the $N_1 - N_2$ plane

can be superimposed to the the SIM (Fig. 14(b)). In general, isolas have higher energy levels causing amplification in the response. More details can be found in [25].

It should be mentioned that the backbone curve [33] of the system can be obtained too from Eq. (64), via setting damping and amplitudes of forcing to zero; for nonlinear conservative systems, this curve provides the amplitude dependency of the frequency.

4. Types of load

To show the capability of the NES to reduce vibrations related to various types of loads, with different frequency contents, some cases are here presented. Loads are resumed in Tab. 1 and shown in Fig. 5 and results reported in Sect. 5.

4.1. Uniform load

A vertical, sinusoidal, uniformly distributed load with frequency Ω_F is applied on the upper flange of the beam (p is in N/m^2). The introduction of non-dimensional time has led to the non-dimensional term Ω , written in Eq. (47). It can be useful to write $\Gamma = \gamma \sin(\Omega\tau)$ where γ can be derived from Tab. 1, so that $\hat{\gamma}$ appearing in Eq. (67) is equal to $\gamma/(2i)$. This case is identified as UL-1.

Moreover, a similar case is considered, but with the load applied only in the mid upper flange of the cross section of the beam, i.e. between the points of intersection of inclined webs with the upper flange, identified as UL-2.

4.2. Punctual load

A vertical, sinusoidal, punctual load with frequency Ω_F is applied at half-length of the beam (p is in N/m , as it has to be written as the ratio between the punctual load in N and the dimension of the element of the cross-section along s). Also in this case $\hat{\gamma}$ is equal to $\gamma/(2i)$. This case is identified as PL.

4.3. Train of moving loads

A train of moving loads, representing a series of N_v vehicles moving on the bridge at constant speed v_V and distance d , is applied on the upper flange of the beam. The frequency of every load is $\Omega_F = n_j \pi v_V / L$ [52]. Expressions in Tab. 1 are meant for each vehicle, where $t_j = (j - 1)d/v_V$ is the arriving time

of the j^{th} load on the beam and $t_j + L/v_V$ is the time when the vehicle leaves the beam. Only the numerical solution of Eqs. (39,40) has been explored using a Runge–Kutta method since, due to the characteristics of the beam, an extremely high speed should be taken to consider a 1:1 resonance, thus resulting in an unrealistic scenario. This case is identified as ML.

4.4. Seismic load

For seismic action, if the NES is disregarded, both analytical and numerical solutions can be obtained, while, for the beam with NES, only the numerical solution of Eqs. (39,40) through a Runge–Kutta method is considered, since it is not possible to apply the aforementioned procedure with a 1:1 resonance, as the earthquake has a wide spectrum of frequencies. Moreover, in general, in Eqs. (27-28) the hypothesis that only the j^{th} vibration mode contributes to the beam response is no more valid and a sufficient number of vibration modes should be considered, and the presence of nonlinear stiffness and damping terms of the NES couples all these vibration modes. However, for the case under study, for the beam without NES it has been seen that, due to the characteristics of the beam itself and of the chosen earthquake, the difference between the analytical solution keeping only the 1st vibration mode, and that with more than one mode is negligible, meaning that for this specific case it is possible to proceed with only one mode.

The earthquake is considered as a vertical ground motion $v_g(t)$, applied to both supports of the beam, so that displacements $v(s, z, t)$ and $y_N(t)$ are relative to the base. As a consequence, the ground acceleration is $\ddot{v}_g(t)$ and, considering the mass per unit area m seen in Eq. (9), the load terms are reported in Tab. 1. This case is identified as SL.

Table 1: Characteristics of different types of loads

Type of load	$f_y(s, z, t)$	\mathbf{p}_Ω^0	$\varepsilon\Gamma$ for $n_j = 1, 5, \dots$
Uniform	$p \sin(\Omega_F t)$	$\int_s p \mathbf{V}(s) ds$	$\frac{4}{n_j \pi \omega_j^2 b_1} \frac{\Theta_j^T \mathbf{p}_\Omega^0}{\Theta_j^T \mathbf{M}_j \Theta_j} \sin(\Omega \tau)$
Punctual	$p \sin(\Omega_F t) \delta(z - L/2)$	$\int_s p \mathbf{V}(s) ds$	$\frac{2}{b_1 L \omega_j^2} \frac{\Theta_j^T \mathbf{p}_\Omega^0}{\Theta_j^T \mathbf{M}_j \Theta_j} \sin(\Omega \tau)$
Moving	$p \delta(z - v_V(t - t_j))$	$\int_s p \mathbf{V}(s) ds$	$\frac{2}{b_1 L \omega_j^2} \frac{\Theta_j^T \mathbf{p}_\Omega^0}{\Theta_j^T \mathbf{M}_j \Theta_j} \sin(\Omega(\tau - \tau_j))$
Seismic	$m \ddot{v}_g(t)$	$\int_s m(\mathbf{U}(s) \sin(\alpha) + \mathbf{V}(s) \cos(\alpha)) ds$	$\frac{4}{n_j \pi \omega_j^2 b_1} \frac{\Theta_j^T \mathbf{p}_\Omega^0}{\Theta_j^T \mathbf{M}_j \Theta_j} \ddot{v}_g(t)$

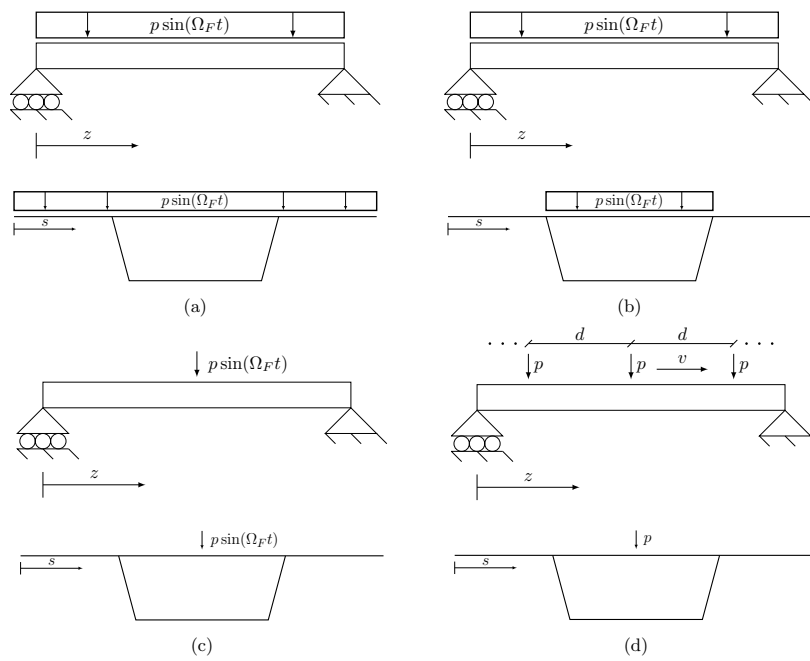


Figure 5: Schematic representation of different types of loads in longitudinal and transversal planes: (a) UL-1, (b) UL-2, (c) PL, (d) ML. Refer to Sect. 4 for definitions of abbreviations.

5. Results

Geometrical and mechanical properties of the beam are presented in Fig. 6 and in Tab. 2, while those of the NES are written in Tab. 3. It should be specified that the choice of the NES parameters does not come from a rigorous optimization procedure [53], so it is plausible that even better results can be found by changing NES properties in terms of efficiency (see for example [19] where different trends of the SIM are identified as the parameters vary.)

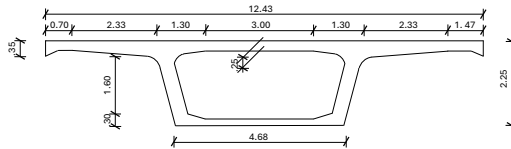


Figure 6: Beam cross-section

Table 2: Geometrical and mechanical properties of the beam

m_{tot} (t)	L (m)	b_1 (m)	ξ_j	E (N/m ²)
571	40.5	3.15	0.1%	3.108×10^{10}

Table 3: Parameters of the NES

m_N (kg)	c_N (Ns/m)	k_N (N/m ³)	z_N (m)
650	2×10^3	6×10^6	$L/2$

In Fig. 7 the analytical SIM, found using Eq. (54), with stability borders (in red), determined in accordance to Eq. (58), is shown together with a numerical solution given by the resolution of Eqs. (39-40) without external load, subjected to some non-trivial initial conditions marked as “x”. The unstable zone is represented by a dashed line and it can be noted that, for these initial conditions, the solution oscillates in time around the second branch and then in correspondence of the stability border jumps on the first branch to go to zero, being the unstable zone physically unattainable.

The backbone curve is showed in Fig. 8 together with some frequency response curves for different load amplitudes in the case UL-1. As it can be seen, it is the locus of the peak amplitudes and it shows that by increasing the amplitude of the external load, the NES performance increases and different kinds of equilibrium points can be obtained.

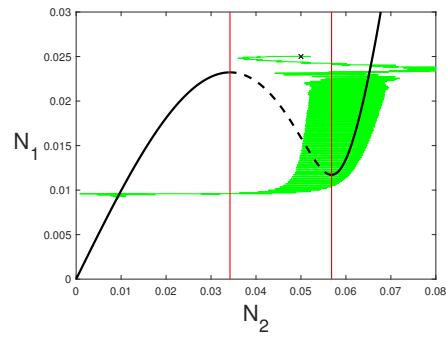


Figure 7: Analytical and numerical SIM

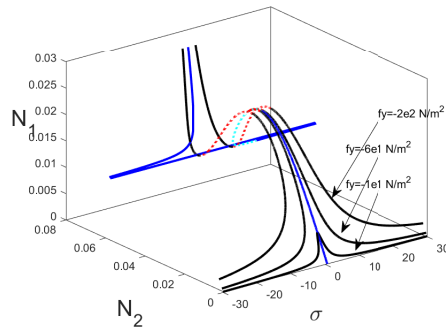


Figure 8: Frequency response curves of the system and backbone curve (in blue and cyan)

5.1. Uniform load

5.1.1. Case 1

A UL-1 case with amplitude $p = 6.0 \times 10^1$ N/m² and frequency equal to that of the first vibration mode (indicated as Φ_1 in Fig. 3) $\Omega_F = \omega_1 = 15.05$ rad/s is considered.

From Fig. 9(a) it can be noticed that for this type of load the NES is well activated and, in Figs. 9(b), 9(c), it is shown that in function of the value of the detuning parameter, it is possible to have 1, 2 or even 3 solutions of different nature, depending on initial conditions. Moreover, in Fig. 9(b) a comparison between frequency response curves of the beam with and without NES highlights a general reduction of displacement on the beam when the nonlinear device is engaged.

Fig. 10(a) shows that for $\sigma = 0.65$ the equilibrium point (represented by the circle) moves in time around the SIM and, when it attains the stability border, it bifurcates, jumping on the other branch. The same behavior, describing a modulated response, can be found in Figs. 10(b), 10(c) where bifurcations in time are evident; furthermore in the same figures N_1 and N_2 are plotted as envelopes of r and a respectively, having the meaning of energies.

In Fig. 11(a) the displacement of the beam and of the NES is shown, normalized with respect to the beam length, while in Fig. 11(b) the response of the beam with and without NES highlights the reduction of its displacement as well as the modulated response.

5.1.2. Case 2

A UL-1 case with amplitude $p = 6.0 \times 10^1$ N/m² and frequency equal to that of the first vibration mode (flexural mode) $\Omega_F = \omega_1 = 15.05$ rad/s with $\sigma = 0$ is considered.

In this case the response is periodic, with the equilibrium point oscillating in time and attaining to an asymptotic value, as showed in Figs. 12(a), 12(b); the values of N_1 and N_2 found solving the numerical problem are almost the same as the analytical ones identified by the vertical line at $\sigma = 0$ in Figs. 9(b), 9(c), highlighting once again the validity of the analytical model. Moreover, in Fig. 13(a), it can be seen that the displacement of the NES is high enough to reduce the displacement of the beam as showed in Fig. 13(b). It should be noticed that, even if the behavior of the NES is not optimal, displacements are compatible with those expected on a real beam.

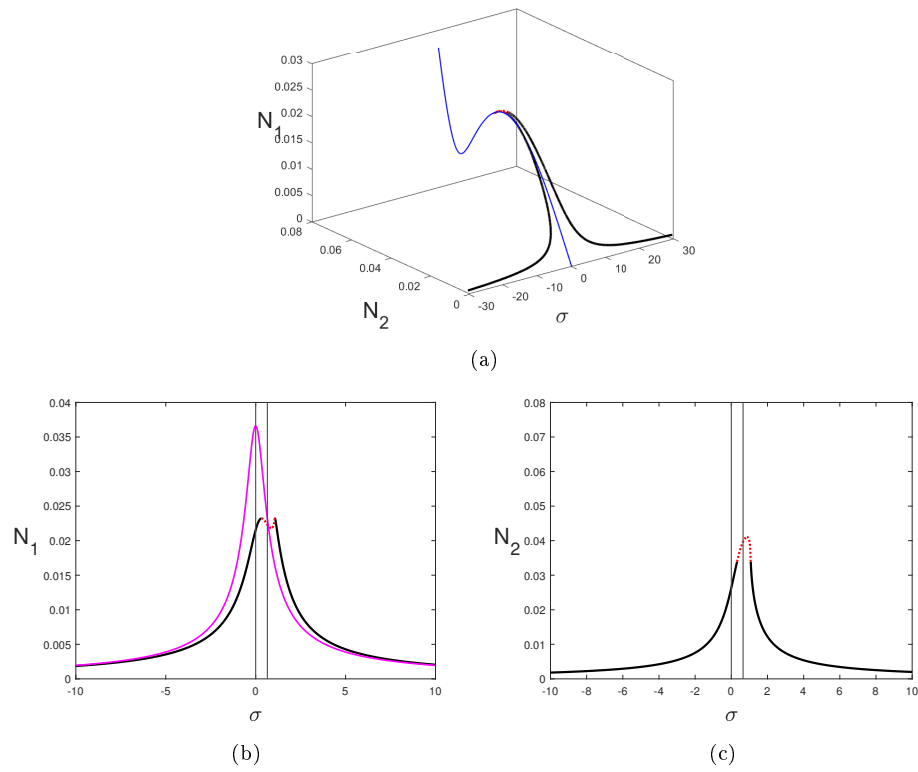
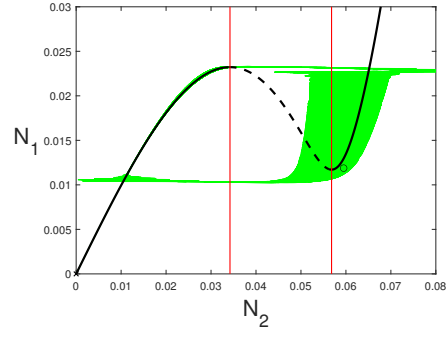
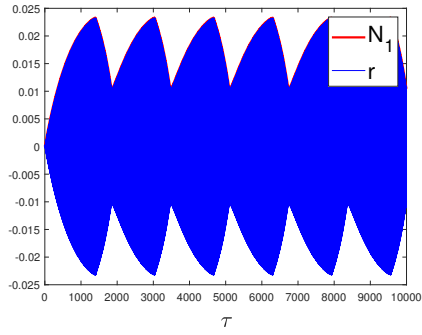


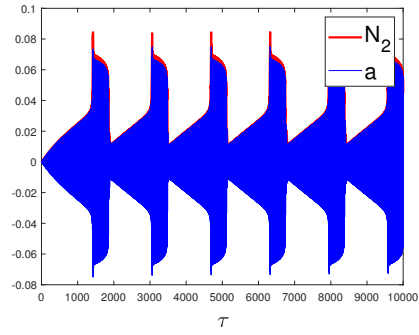
Figure 9: Different views of the frequency response curve for the system under UL-1 load for $p = 6.0 \times 10^1 \text{ N/m}^2$: (a) Three dimensional view in $N_1 - N_2 - \sigma$ (the unstable zone of the SIM is showed in dashed red) with SIM (in blue); (b) Two dimensional view in $N_1 - \sigma$ with the frequency response curve of the beam without NES (in magenta); (c) Two dimensional view in $N_2 - \sigma$. Vertical lines represent values of σ investigated in next Figures



(a)



(b)



(c)

Figure 10: SIM and numerical results for the system under UL-1 load for $p = 6.0 \times 10^1 \text{ N/m}^2$, $\sigma = 0.65$: (a) $N_1 - N_2$ with SIM ; (b) Time history of N_1 and r ; (c) Time history of N_2 and a . Numerical results are obtained from direct numerical integration of Eqs. (39-40) with zero initial conditions

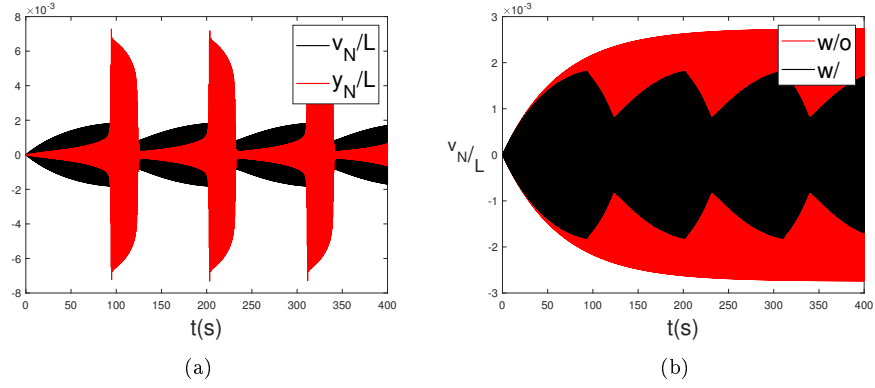


Figure 11: Numerical results for the system under UL-1 load for $p = 6.0 \times 10^1 \text{ N/m}^2$, $\sigma = 0.65$: (a) Time histories of v_N/L and y_N/L ; (b) Time histories of v_N/L with and without NES. Numerical results are obtained from direct numerical integration of Eqs. (39-40) with zero initial conditions

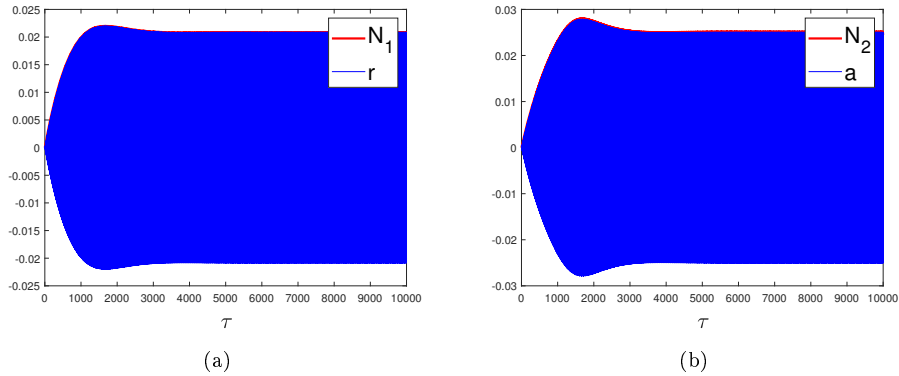


Figure 12: Numerical results for the system under UL-1 load for $p = 6.0 \times 10^1 \text{ N/m}^2$, $\sigma = 0$: (a) Time history of N_1 and r ; (b) Time history of N_2 and a . Numerical results are obtained from direct numerical integration of Eqs. (39-40) with zero initial conditions

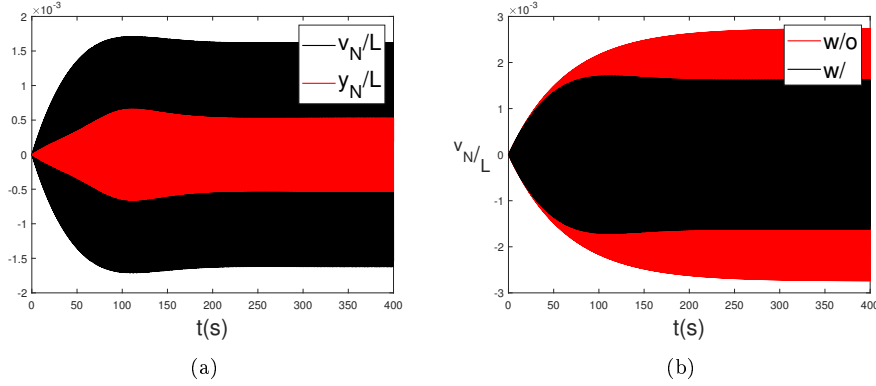


Figure 13: Numerical results for the system under UL-1 load for $p = 6.0 \times 10^1$ N/m², $\sigma = 0$: (a) Time histories of v_N/L and y_N/L ; (b) Time histories of v_N/L with and without NES. Numerical results are obtained from direct numerical integration of Eqs. (39-40) with zero initial conditions

5.1.3. Case 3

A UL-2 case with amplitude $p = 2.0 \times 10^4$ N/m² and frequency equal to that of the fifth vibration mode (indicated as Φ_5 in Fig. 3) $\Omega_F = \omega_5 = 87.21$ rad/s is considered.

Results reported in Figs. 14(a), 14(b), 14(c) are quite interesting, since they show the onset on an isola (see for example [54, 55]), which can be dangerous for the beam due to the higher energy level (note that stable and unstable zones are referred to those of the SIM). Figs. 15(a), 15(b) show once again the excellent correspondence of the numerical solution and the analytical one, as can be seen by looking at the values intercepted by the vertical lines in Fig. 14(c). Moreover, in Figs. 16(a), 16(b) the reduction of the displacement on the beam, thanks to the Modulated Response of the NES is still evident, meaning that the same NES can be used to control a different type of load with different frequency, which has been detected thanks to GBT: in fact, it should be underlined that in this case GBT is fundamental to detect this vibration mode, which, as can be seen in Fig. 3, exhibits the deformation of the cross-section in its own plane.

5.2. Punctual load

A PL case with amplitude $p = 3.0 \times 10^4$ N (divided by the the dimension of the cross-section element along s to have a load for unit length) and frequency equal to that of the first vibration mode is considered.

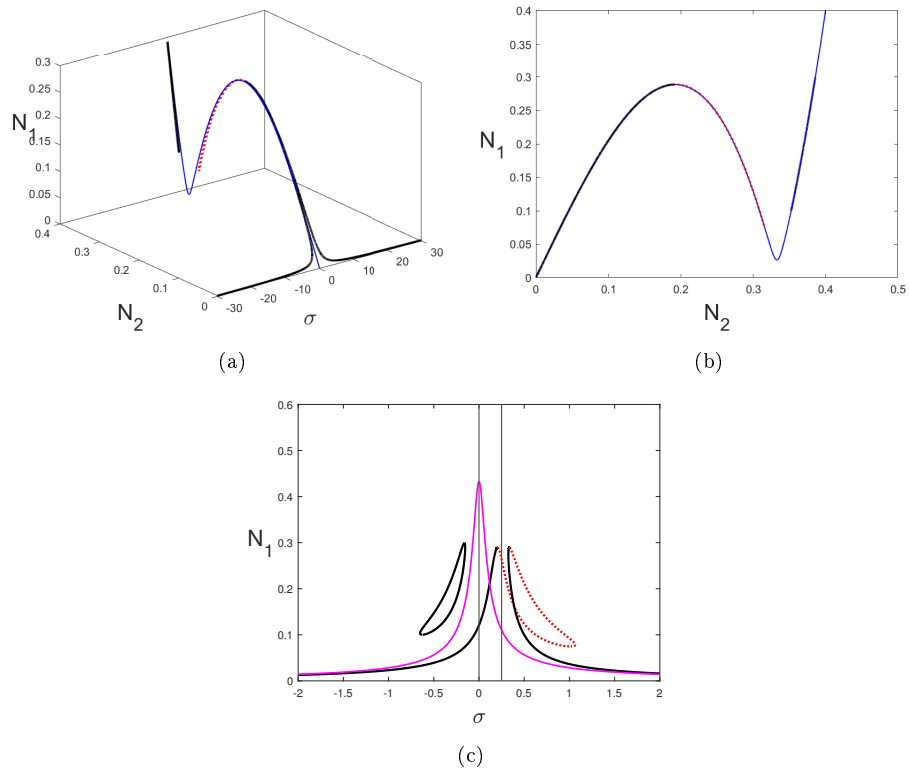


Figure 14: Different views of the frequency response curve for the system under UL-2 load for $p = 2.0 \times 10^4$ N/m²: (a) Three dimensional view in $N_1 - N_2 - \sigma$ (the unstable zone of the SIM is showed in dashed red) with SIM (in blue); (b) Two dimensional view in $N_1 - N_2$ with SIM; (c) Two dimensional view in $N_1 - \sigma$ with the frequency response curve of the beam without NES (in magenta). Vertical lines represent values of σ investigated in next Figures

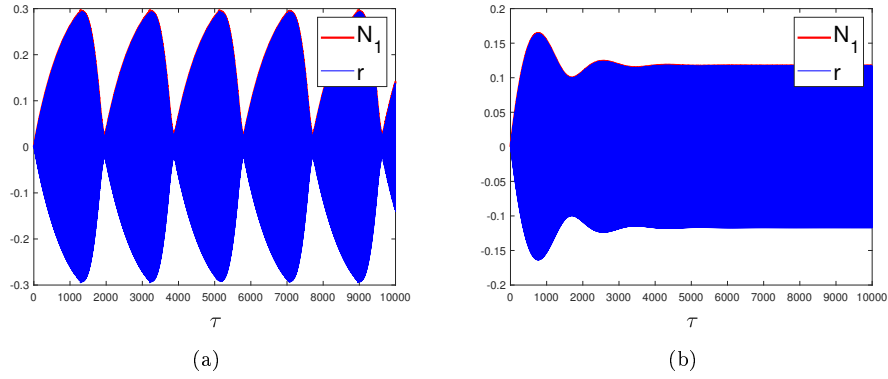


Figure 15: Numerical results for the system under UL-2 load for $p = 2.0 \times 10^4$ N/m²: (a) Time history of N_1 and r for $\sigma = 0.25$; (c) Time history of N_1 and r for $\sigma = 0$. Numerical results are obtained from direct numerical integration of Eqs. (39-40) with zero initial conditions

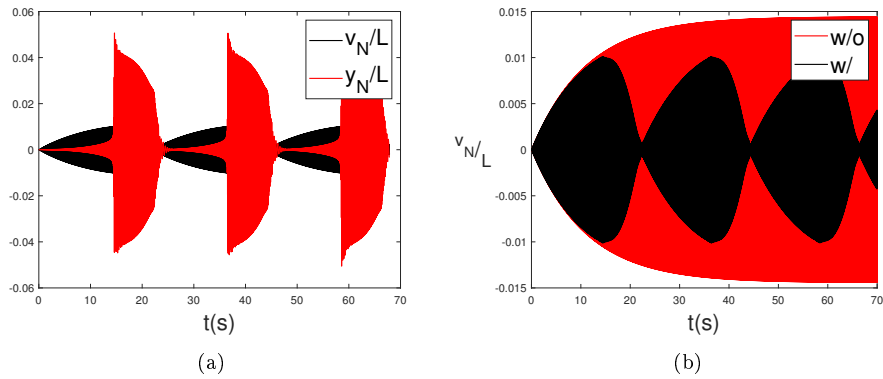


Figure 16: Numerical results for the system under UL-2 load for $p = 2.0 \times 10^4$ N/m², $\sigma = 0.25$: (a) Time histories of v_N/L and y_N/L ; (b) Time histories of v_N/L with and without NES. Numerical results are obtained from direct numerical integration of Eqs. (39-40) with zero initial conditions

Results are qualitatively the same of those shown for uniform load, as can be seen in Fig. 17(a) where the isola is also present, and in Fig. 17(b), showing the ability of the NES to reduce vibrations on this type of beam also for this type of load.

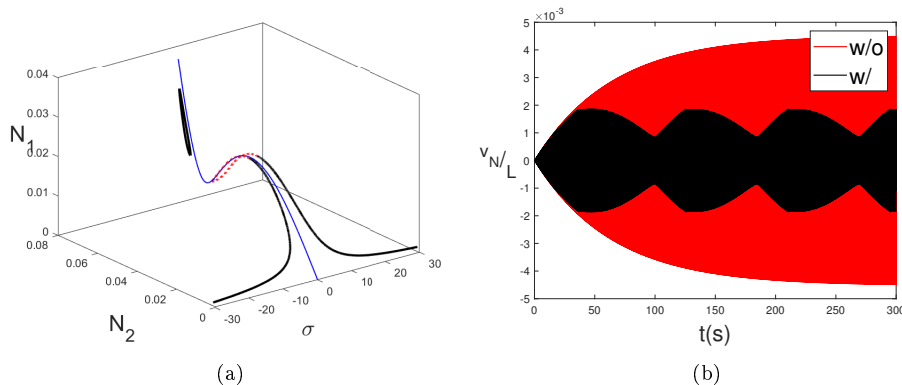


Figure 17: (a) Three dimensional view of the frequency response curve for the system under PL load for $p = 3.0 \times 10^4$ N (the unstable zone of the SIM is showed in dashed red) with SIM (in blue); (b) Time histories of v_N/L with and without NES for $\sigma = 0.5$. Numerical results are obtained from direct numerical integration of Eqs. (39-40) with zero initial conditions

5.3. Train of moving loads

Different combinations of parameters can be considered for this type of load. In this case $N_v = 80$ vehicles, at a distance $d = 20$ m with a speed $v_V = 70$ m/s and with amplitude $p = 3.0 \times 10^5$ N is considered.

Results reported in Figs. 18(a), 18(b) show a reduction of the vertical displacement of the beam with NES, both during the transit of vehicles on the bridge and in free oscillations. Even though the NES is activated, the reduction is not so impressive in this case, and it can be better appreciated in the tail of the Figures, when all the vehicles have passed through the beam; it is likely that the high number of parameters involved for the load, in addition to those of the NES, do not permit an ideal reduction in vibrations. In Tabs. 4-5 some results are reported, showing the influence of different vehicle parameters on vibration control; values are $(v_N^{w/} - v_N^{w/o})/v_N^{w/o}$ in percentage. In particular, from Tab. 4 it can be noticed that if vehicles are too close or too far, with respect to the beam length, the NES could increase the displacement (positive difference) rather than reducing it, above all for higher speed values.

On the other hand, Tab. 5 shows that for some combinations of N_v and v_V the reduction is more effective. Furthermore, it should be stated that the chosen speed of vehicles is quite far from the critical one, which for the characteristics of this beam is too high to have a physical meaning, so the reduction may not be optimal.

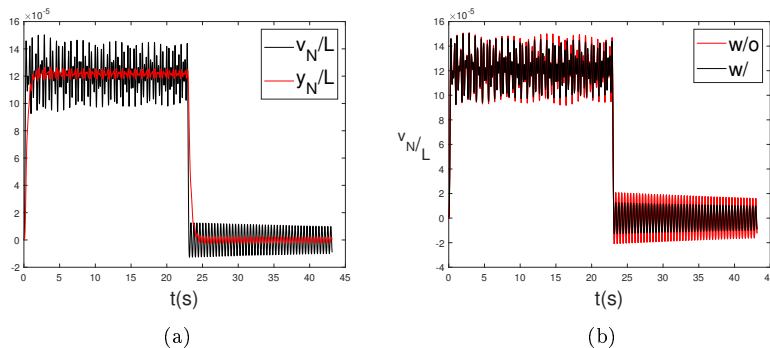


Figure 18: Numerical results for the system under ML load for $p = 3.0 \times 10^5$ N/m², $N_v = 80$, $d = 20$ m, $v_V = 70$ m/s: (a) Time histories of v_N/L and y_N/L ; (b) Time histories of v_N/L with and without NES. Numerical results are obtained from direct numerical integration of Eqs. (39-40) with zero initial conditions

Table 4: Influence of d and v_V on vibrations reduction with $p = 3.0 \times 10^5$ N/m² and $N_v = 80$. Values represent $(v_N^{w/} - v_N^{w/o})/v_N^{w/o}$ in percentage

$v_V \backslash d$	d		
	15 (m)	20 (m)	30 (m)
36 (m/s)	-4.56	-29.41	-0.23
50 (m/s)	-6.25	-15.88	+30.12
70 (m/s)	+44.75	-38.85	+22.92

5.4. Seismic load

A SL case has been considered with $\ddot{v}_g(t)$ taken as the time history of a past earthquake (L'Aquila, 2009), chosen such that the range of frequencies of the event, identified by its spectrum, was around the 1st frequency of the beam, with a vertical PGA, slightly increased, of 0.52 g (Fig. 19(a)). Numerical results shown in Figs. 19(b), 19(c), highlight the instant when the NES is activated, almost corresponding to the moment when the seismic acceleration reaches its peak value, and show an evident reduction of displacement of

Table 5: Influence of N_v and v_V on vibrations reduction with $p = 3.0 \times 10^5$ N/m² and $d = 20$ m. Values represent $(v_N^{w/} - v_N^{w/o})/v_N^{w/o}$ in percentage

$N_v \backslash v_V$	10	20	50
36 (m/s)	-2.71	-6.90	-24.79
50 (m/s)	-2.06	+7.34	-28.49
70 (m/s)	-9.25	-13.43	+1.29

the beam with the NES, even if the maximum displacement is not reduced. This application demonstrates the validity of the NES in reducing vibrations related to real loading scenarios, which can otherwise cause severe problems on bridge decks.

6. Conclusions

A full-scale beam has been studied with the goal of reducing vibrations caused by different types of loads with different frequencies. Due to its shape, the beam has been modeled through Generalized Beam Theory to take into account aspects like the deformation of the cross-section in its own plane and to consider vibration modes (like torsional, local or mixed ones) which cannot be considered with simpler beam theories. The beam, linked to a Nonlinear Energy Sink, has been studied through the Complexification Averaging Method, highlighting a good reduction in beam vibrations for 1:1 resonant loads, with different behaviors (periodic, modulated response, isolas). A lower reduction for non-resonant loads has been shown, like earthquake or train of moving loads.

Possible future developments include an optimization analysis to find the best parameters for the Nonlinear Energy Sink, the use of different types of nonlinearities (e.g. non-smooth ones) for the device and the implementation of geometrical and mechanical nonlinearities in the beam model.

CRedit authorship contribution statement

Andrea De Flaviis: Conceptualization, Data curation, Formal analysis, Investigation, Methodology, Software, Resources, Validation, Visualization, Writing – original draft, Writing – review & editing. **Alireza Ture**

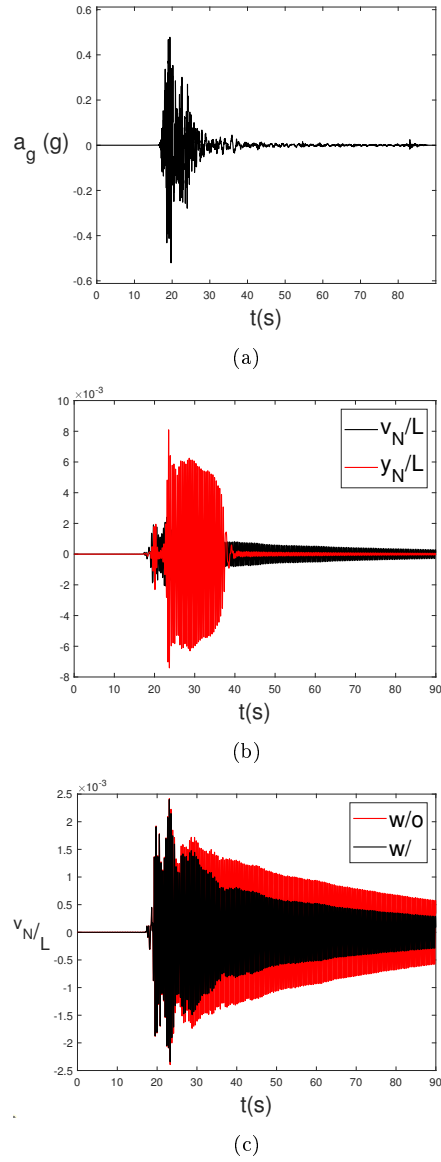


Figure 19: Numerical results for the system under SL load: (a) Time history of the event; (b) Time histories of v_N/L and y_N/L ; (c) Time histories of v_N/L with and without NES. Numerical results are obtained from direct numerical integration of Eqs. (39-40) with zero initial conditions

Savadkoochi: Conceptualization, Investigation, Methodology, Project administration, Resources, Supervision, Validation, Writing – review & editing. **Daniele Zulli:** Conceptualization, Funding acquisition, Investigation, Methodology, Project administration, Resources, Supervision, Validation, Writing – review & editing.

Declaration of interests

The authors have no relevant financial or non-financial interests to disclose.

Funding sources

The first author has received research support from Company “Dimensione Solare S.r.l.” as part of the financial program of his PhD thesis.

Data Availability

The datasets generated during and/or analyzed during the current study are available from the corresponding author on request.

References

- [1] H. Frahm, Device for damping vibrations of bodies., US Patent 989,958 (1911).
- [2] J. P. Den Hartog, Mechanical Vibrations., McGraw-Hill Book Company, New York and London, 1947.
- [3] T. Ioi, K. Ikeda, On the Dynamic Vibration Damped Absorber of the Vibration System., Bulletin of JSME 21 (151) (1978) 64–71. doi:10.1299/jsme1958.21.64.
- [4] Y. Fujino, M. Abé, Design formulas for tuned mass dampers based on A perturbation technique., Earthquake Engineering & Structural Dynamics 22 (10) (1993) 833–854. doi:10.1002/eqe.4290221002.
- [5] A.-P. Wang, R.-F. Fung, S.-C. Huang, Dynamic analysis of a tall building with a tuned-mass-damper device subjected to earthquake excitations., Journal of Sound and Vibration 244 (1) (2001) 123–136. doi:10.1006/jsvi.2000.3480.

- [6] V. Gattulli, F. Di Fabio, A. Luongo, Simple and double Hopf bifurcations in aeroelastic oscillators with tuned mass dampers., *Journal of the Franklin Institute* 338 (2) (2001) 187–201. doi:10.1016/S0016-0032(00)00077-6.
- [7] S. V. Bakre, R. S. Jangid, Optimum parameters of tuned mass damper for damped main system., *Structural Control and Health Monitoring* 14 (3) (2007) 448–470. doi:10.1002/stc.166.
- [8] A. Casalotti, A. Arena, W. Lacarbonara, Mitigation of post-flutter oscillations in suspension bridges by hysteretic tuned mass dampers., *Engineering Structures* 69 (2014) 62–71. doi:10.1016/j.engstruct.2014.03.001.
- [9] R. E. Roberson, Synthesis of a nonlinear dynamic vibration absorber., *Journal of the Franklin Institute* 254 (3) (1952) 205–220. doi:10.1016/0016-0032(52)90457-2.
- [10] O. Gendelman, L. I. Manevitch, A. F. Vakakis, R. M’Closkey, Energy Pumping in Nonlinear Mechanical Oscillators: Part I—Dynamics of the Underlying Hamiltonian Systems., *Journal of Applied Mechanics* 68 (1) (2000) 34–41. doi:10.1115/1.1345524.
- [11] O. Gendelman, Y. Starosvetsky, M. Feldman, Attractors of harmonically forced linear oscillator with attached nonlinear energy sink I: Description of response regimes., *Nonlinear Dynamics* 51 (2008) 31–46. doi:10.1007/s11071-006-9167-0.
- [12] O. V. Gendelman, Y. Starosvetsky, Quasi-Periodic Response Regimes of Linear Oscillator Coupled to Nonlinear Energy Sink Under Periodic Forcing., *Journal of Applied Mechanics* 74 (2) (2006) 325–331. doi:10.1115/1.2198546.
- [13] Y. Starosvetsky, O. Gendelman, Strongly modulated response in forced 2DOF oscillatory system with essential mass and potential asymmetry., *Physica D: Nonlinear Phenomena* 237 (13) (2008) 1719–1733. doi:10.1016/j.physd.2008.01.019.
- [14] Y. Starosvetsky, O. Gendelman, Response regimes in forced system with non-linear energy sink: quasi-periodic and random forcing., *Nonlinear Dynamics* 64 (2011) 177–195. doi:10.1007/s11071-010-9856-6.

- [15] D. Zulli, A. Luongo, Control of primary and subharmonic resonances of a Duffing oscillator via non-linear energy sink., *International Journal of Non-Linear Mechanics* 80 (2016) 170–182. doi:10.1016/j.ijnonlinmec.2015.08.014.
- [16] B. Vaurigaud, A. Ture Savadkoohi, C.-H. Lamarque, Targeted energy transfer with parallel nonlinear energy sinks. Part I: Design theory and numerical results., *Nonlinear Dynamics* 66 (2011) 763–780. doi:10.1007/s11071-011-9949-x.
- [17] A. F. Vakakis, O. V. Gendelman, L. A. Bergman, D. M. McFarland, G. Kerschen, Y. S. Lee, *Nonlinear targeted energy transfer in mechanical and structural systems I & II*, Springer, Germany, 2008.
- [18] E. Gourdon, C.-H. Lamarque, Energy Pumping with Various Nonlinear Structures: Numerical Evidences., *Nonlinear Dynamics* 40 (2005) 281–307. doi:10.1007/s11071-005-6610-6.
- [19] C.-H. Lamarque, O. Gendelman, A. Ture Savadkoohi, E. Etcheverria, Targeted energy transfer in mechanical systems by means of non-smooth nonlinear energy sink., *Acta Mechanica* 221 (2011) 175–200. doi:10.1007/s00707-011-0492-0.
- [20] H. Ding, L.-Q. Chen, Designs, analysis, and applications of nonlinear energy sinks., *Nonlinear Dynamics* 100 (2020) 3061–3107. doi:10.1007/s11071-020-05724-1.
- [21] A. Saeed, R. Abdul Nasar, M. AL-Shudeifat, A review on nonlinear energy sinks: designs, analysis and applications of impact and rotary types., *Nonlinear Dynamics* 111 (2023) 1–37. doi:10.1007/s11071-022-08094-y.
- [22] G. Hurel, A. Ture Savadkoohi, C.-H. Lamarque, Nonlinear Vibratory Energy Exchanges between a Two-Degree-of-Freedom Pendulum and a Nonlinear Absorber., *Journal of Engineering Mechanics* 145 (8) (2019) 04019058. doi:10.1061/(ASCE)EM.1943-7889.0001620.
- [23] G. Hurel, A. Ture Savadkoohi, C.-H. Lamarque, Passive control of a two degrees-of-freedom pendulum by a non-smooth absorber., *Nonlinear dynamics* 98 (2019) 3025–3036. doi:10.1007/s11071-019-04891-0.

- [24] L. Leroux, S. Langlois, A. Ture Savadkoohi, Investigation of a nonlinear control of galloping with a linear beam with elastic boundary conditions., *International Journal of Non-Linear Mechanics* 156 (2023) 104484. doi: 10.1016/j.ijnonlinmec.2023.104484.
- [25] C. da Silveira Zanin, A. Ture Savadkoohi, S. Baguet, R. Dufour, G. Hurel, Nonlinear vibratory energy exchanges in a meta-cell., *International Journal of Non-Linear Mechanics* 146 (2022) 104148. doi: 10.1016/j.ijnonlinmec.2022.104148.
- [26] Y. Chen, Z. Qian, K. Chen, P. Tan, S. Tesfamariam, Seismic performance of a nonlinear energy sink with negative stiffness and sliding friction., *Structural Control and Health Monitoring* 26 (11) (2019) e2437. doi:10.1002/stc.2437.
- [27] F. Georgiades, A. Vakakis, Dynamics of a linear beam with an attached local nonlinear energy sink., *Communications in Nonlinear Science and Numerical Simulation* 12 (5) (2007) 643–651. doi:10.1016/j.cnsns.2005.07.003.
- [28] D. Zulli, A. Luongo, Non linear energy sink to control vibrations of an internally non resonant elastic string., *Meccanica* 50 (2015) 781–794. doi:10.1007/s11012-014-0057-0.
- [29] A. Luongo, D. Zulli, Nonlinear energy sink to control elastic strings: the internal resonance case., *Nonlinear Dynamics* 81 (2015) 425–435. doi:10.1007/s11071-015-2002-8.
- [30] Y.-W. Zhang, S. Hou, Z. Zhang, J. Zang, Z.-Y. Ni, Y.-Y. Teng, L.-Q. Chen, Nonlinear vibration absorption of laminated composite beams in complex environment., *Nonlinear Dynamics* 99 (2020) 2605–2622. doi: 10.1007/s11071-019-05442-3.
- [31] Y. Wang, H. Kang, Y. Cong, T. Guo, W. Zhu, Vibration suppression of a cable under harmonic excitation by a nonlinear energy sink, *Communications in Nonlinear Science and Numerical Simulation* 117 (2023) 106988. doi:10.1016/j.cnsns.2022.106988.
- [32] L. Manevitch, The Description of Localized Normal Modes in a Chain of Nonlinear Coupled Oscillators Using Complex Variables., *Nonlinear Dynamics* 25 (2001) 95–109. doi:10.1023/A:1012994430793.

- [33] A. Nayfeh, D. Mook, *Nonlinear Oscillations.*, John Wiley & Sons, New York, 1995.
- [34] A. Ture Savadkoohi, C.-H. Lamarque, M. Weiss, B. Vaurigaud, S. Charlemagne, Analysis of the 1:1 resonant energy exchanges between coupled oscillators with rheologies., *Nonlinear Dynamics* 86 (4) (2016) 2145–2159. doi:10.1007/s11071-016-2792-3.
- [35] A. Luongo, D. Zulli, Dynamic analysis of externally excited NES-controlled systems via a mixed Multiple Scale/Harmonic Balance algorithm., *Nonlinear Dynamics* 70 (2012) 2049–2061. doi:10.1007/s11071-012-0597-6.
- [36] A. Luongo, D. Zulli, Aeroelastic instability analysis of NES-controlled systems via a mixed multiple scale/harmonic balance method., *Journal of Vibration and Control* 20 (13) (2014) 1985–1998. doi:10.1177/1077546313480542.
- [37] R. Schardt, Eine Erweiterung der Technischen Biegetheorie zur Berechnung prismatischer Faltwerke., *Der Stahlbau* 35 (1966) 161–171, (In German).
- [38] R. Schardt, Generalized beam theory—an adequate method for coupled stability problems., *Thin-Walled Structures* 19 (2) (1994) 161–180. doi:10.1016/0263-8231(94)90027-2.
- [39] J. Davies, P. Leach, Some applications of Generalized Beam Theory., *international Specialty Conference on Cold-Formed Steel Structures*. 2. (1992).
- [40] J. Davies, P. Leach, First-order Generalised Beam Theory., *Journal of Constructional Steel Research* 31 (2) (1994) 187–220. doi:10.1016/0143-974X(94)90010-8.
- [41] N. Silvestre, D. Camotim, First-order generalised beam theory for arbitrary orthotropic materials., *Thin-Walled Structures* 40 (9) (2002) 755–789. doi:10.1016/S0263-8231(02)00025-3.
- [42] N. Silvestre, D. Camotim, Nonlinear Generalized Beam Theory for Cold-formed Steel Members., *International Journal of Structural Stability and Dynamics* 3 (4) (2003) 461–490. doi:10.1142/S0219455403001002.

- [43] R. Bebiano, R. Gonçalves, D. Camotim, A cross-section analysis procedure to rationalise and automate the performance of gbt-based structural analyses., *Thin-Walled Structures* 92 (2015) 29–47. doi:10.1016/j.tws.2015.02.017.
- [44] D. Camotim, N. Silvestre, C. Basaglia, R. Bebiano, Gbt-based buckling analysis of thin-walled members with non-standard support conditions., *Thin-Walled Structures* 46 (7-9) (2008) 800–815. doi:10.1016/j.tws.2008.01.019.
- [45] R. Gonçalves, D. Camotim, C. Basaglia, A. Martins, N. Peres, Latest developments on the analysis of thin-walled structures using Generalised Beam Theory (GBT)., *Journal of Constructional Steel Research* 204 (2023) 107858. doi:10.1016/j.jcsr.2023.107858.
- [46] G. Ranzi, A. Luongo, A new approach for thin-walled member analysis in the framework of GBT., *Thin-Walled Structures* 49 (11) (2011) 1404–1411. doi:10.1016/j.tws.2011.06.008.
- [47] G. Piccardo, G. Ranzi, A. Luongo, A complete dynamic approach to the Generalized Beam Theory cross-section analysis including extension and shear modes., *Mathematics and Mechanics of Solids* 19 (8) (2013) 900–924. doi:10.1177/1081286513493107.
- [48] A. De Flaviis, R. Alaggio, D. Zulli, Generalized Beam Theory for the static and dynamic response of a bridge deck with Structural Health Monitoring purposes, *Procedia Structural Integrity* 62 (2024) 871–878. doi:10.1016/j.prostr.2024.09.117.
- [49] R. Bebiano, D. Camotim, N. Silvestre, Dynamic analysis of thin-walled members using Generalised Beam Theory (GBT)., *Thin-Walled Structures* 72 (2013) 188–205. doi:10.1016/j.tws.2013.07.004.
- [50] H. Troger, A. Steindl, *Nonlinear Stability and Bifurcation Theory. An Introduction for Engineers and Applied Scientists*, Springer-Verlag/Wien, New York, 1991.
- [51] J. Carr, *Applications of Centre Manifold Theory.*, Vol. 35, Applied Mathematical Sciences. Springer-Verlag, New York - Heidelberg - Berlin, 1981. doi:10.1007/978-1-4612-5929-9.

- [52] Y. Yang, J. Yau, Y. Wu, *Vehicle–Bridge Interaction Dynamics*, World Scientific, 2004.
- [53] E. Boroson, S. Missoum, P.-O. Mattei, C. Vergez, Optimization under uncertainty of parallel nonlinear energy sinks, *Journal of Sound and Vibration* 394 (2017) 451–464. doi:10.1016/j.jsv.2016.12.043.
- [54] H. Guo, T. Yang, Y. Chen, L.-Q. Chen, Singularity analysis on vibration reduction of a nonlinear energy sink system, *Mechanical Systems and Signal Processing* 173 (2022) 109074. doi:10.1016/j.ymsp.2022.109074.
- [55] R. Kuether, L. Renson, T. Detroux, C. Grappasonni, G. Kerschen, M. Allen, Nonlinear normal modes, modal interactions and isolated resonance curves, *Journal of Sound and Vibration* 351 (2015) 299–310. doi:10.1016/j.jsv.2015.04.035.